European Polymer Journal 217 (2024) 113315

Contents lists available at ScienceDirect

European Polymer Journal

journal homepage: www.elsevier.com/locate/europolj

Research Insights

Synthesis of Polyimide-PEO Copolymers: Toward thermally stable solid polymer electrolytes for Lithium-Metal batteries

Timofey I. Kolesnikov [a,b], Dominik Voll [b], Fabian Jeschull [a,*], Patrick Theato [b,c,**]

[a] Karlsruhe Institute of Technology (KIT), Institute for Applied Materials - Energy Storage Systems (IAM-ESS), Hermann-von-Helmholtz-Platz 1, Eggenstein-Leopoldshafen 76344, Germany
[b] Karlsruhe Institute of Technology (KIT), Institute for Chemical Technology and Polymer Chemistry (ITCP), Engesserstraße 18, Karlsruhe 76131, Germany
[c] Karlsruhe Institute of Technology (KIT), Soft Matter Synthesis Laboratory - Institute for Biological Interfaces III (IBG-3), Hermann-von-Helmholtz-Platz 1, Eggenstein-Leopoldshafen 76344, Germany

ARTICLE INFO

Keywords:
Solid polymer electrolyte
PEO
Polyimide
Ionic conductivity

ABSTRACT

The rapid pace of technological advancement in field of electric vehicles and need in sustainable energy sources calls for new, high-performance energy storage technologies. Lithium metal batteries (LMBs) based on solid polymer electrolyte represent a promising battery technology to increase energy density of conventional batteries while enhancing safety, eliminating dendrite formation, and providing mechanical flexibility. In this study, we developed novel polyimide-poly(ethylene oxide) (PI-PEO) copolymers and employed them as solid polymer electrolytes for LMBs. Copolymers with 5, 15, and 30 mol% of PEO-containing diamine were synthesized by reacting with aromatic dianhydride and diamine, using a facile and eco-friendly method in a benzoic acid melt. Chemical structures were confirmed using NMR and IR spectroscopy. Glass transition temperatures varied from 24 °C to 195 °C, increasing with a decrease in the PEO/PI moiety ratio. All copolymers demonstrated good thermal stability up to $T_{5\%} > 345$ °C with a two-step degradation and favorable mechanical properties below the glass transition temperature, as observed by DMA measurements. Solid polymer electrolytes with 70 wt% of LiTFSI exhibited an ionic conductivity of 1.4×10^{-4} S cm^{-1} at 70 °C, with a transference number of 0.7. The polymer electrolyte exhibited non-flammable properties and the potential for utilization in lithium metal batteries, indicating the promising application of these new polymers for high-safety battery systems.

1. Introduction

Lithium-ion batteries (LIBs) are the most ubiquitous technology used currently in energy storage for portable electronic devices and electric vehicles. The need to enhance performance and safety has driven the development of new materials for use in LIBs [1]. While traditional liquid electrolytes in LIBs offer high efficiency, concerns about their safety, such as toxicity, flammability, and leakage, underscore the imperative to develop new electrolytes [2]. Polymer electrolytes are promising candidates due to their potential to enhance safety by eliminating volatile and flammable liquid electrolytes. Additionally, they offer good processability, high mechanical and thermal properties, and lightweight characteristics [3–8]. Furthermore, the utilization of solid polymer electrolytes allows for the development of dendrite-free LMBs with higher theoretical capacity (3860 mAh/g) and improved safety in comparison with LIBs [9–11].

Generally, solid polymer electrolytes (SPEs) consist of a polymer matrix and an ion-conducting salt dissolved in the polymer [12]. Among all polymers that have been studied as SPEs, poly(ethylene oxide) (PEO) clearly stands out and has been most extensively studied [13–15]. The ionic conductivity of PEO was first discovered by Wright in the 1970 s, attributed to the high solvation power provided by ether coordination sites [16,17]. Armand further advanced this research in the 1980 s by successfully utilizing PEO polymer electrolytes in electrochemical devices [18]. In the 2000 s, batteries utilizing PEO-based SPE were commercialized by the Bolloré group, employing lithium metal anodes

* Corresponding author at: Karlsruhe Institute of Technology (KIT), Institute for Applied Materials - Energy Storage Systems (IAM-ESS), Hermann-von-Helmholtz-Platz 1, Eggenstein-Leopoldshafen 76344, Germany.
** Corresponding author at: Karlsruhe Institute of Technology (KIT), Institute for Chemical Technology and Polymer Chemistry (ITCP), Engesserstraße 18, Karlsruhe 76131, Germany.
E-mail addresses: fabian.jeschull@kit.edu (F. Jeschull), patrick.theato@kit.edu (P. Theato).

https://doi.org/10.1016/j.eurpolymj.2024.113315
Received 24 May 2024; Received in revised form 11 July 2024; Accepted 17 July 2024
Available online 19 July 2024

and lithium iron phosphate (LFP) cathodes that allowed operation at temperatures ranging between 60 and 80 °C [19]. Despite this first application, there is still room for improvement of polymer electrolytes in terms of ionic conductivity, electrochemical stability, mechanical and thermal properties. PEO possess a low glass transition temperature and a good salt solvation ability. However, it is semi-crystalline polymer in which ionic transport mainly occurs in the amorphous phase, resulting in low ionic conductivity at temperatures below its melting point of around 70 °C. With increasing temperatures, the crystalline domains melt, leading to a dramatic drop in mechanical properties, but a notable increase in ionic conductivity. Various strategies have been successfully employed to decrease the crystallization degree of PEO and improve the mechanical properties, such as by copolymerization [20,21], blending [22–24], crosslinking [25–27] and introduction of nanoparticles [28–30]. For example, PEO was copolymerized using radical polymerization with polystyrene [31–33], polyacrylonitrile [34], methacrylic sulfonamide [35] or ring opening polymerization with poly(ε-caprolactone) [36], poly(iminoethylene) [37], poly(lactic acid) [20]. However, presence of regular structures and long PEO chains still lead to the presence of a crystalline phase. Copolymerization of PEO with polybenzoxazine by Wang *et al.* [38] using polycondensation resulted in a completely amorphous polymer with good mechanical properties that was successfully utilized for LMB. Additionally, polycondensation is known for its random distribution of functional units, often resulting in an amorphous structure [39]. Therefore, synthesis of PEO containing copolymers using polycondensation might lead to completely amorphous polymers with good mechanical properties and high ionic conductivity.

Aromatic polyimides (PI) stand out as one of the most heat-resistant high-performance polymers, characterized by outstanding mechanical properties, excellent thermal stability, fire and insulation resistance, and high chemical stability in aggressive environments [40–44]. These properties make them indispensable not only in advanced aircraft and airspace industries, but also in energy storage devices [45,46], where they serve as binders [47,48], separators [49], redox-active materials [50–52], coatings [53], nanofiber [54,55] and electrolytes [56–58]. Various PEO-PI copolymers have been previously synthesized for applications in gas separation [59,60], electrode redox-active materials [48,51], binders [48], dielectric film capacitors [61], and fuel cells [62–64], exhibiting an amorphous structure and excellent thermal stability. Consequently, the high thermal and mechanical stability of PI, coupled with the good solvation ability and ionic conductivity of PEO, suggests that a novel class of amorphous polymer electrolyte may be a promising candidate for high-temperature LMBs.

In this study, new PI-PEO copolymers with various block ratios were synthesized *via* polycondensation reaction. The structure–property relationship was characterized for their thermal, mechanical and electrochemical properties. An optimized copolymer formulation was used as SPE in a LMB and examined over 50 cycles, demonstrating its potential use as a non-flammable solid polymer electrolyte.

2. Experimental

2.1. Materials

Jeffamine ED-2003, 4,4′-(hexafluoroisopropylidene)diphthalic anhydride (99 %) (6FDA), benzoic acid (≥99.5 %), 4,4′-(hexafluoroisopropylidene)bis(*p*-phenyleneoxy)dianiline (97 %) (HFBAPP) were purchased from Sigma-Aldrich (USA). Bis(trifluoromethane)sulfonimide lithium salt (LiTFSI, 99.95 %, ABCR) and acetone, anhydrous (≥99.8 % max. 0.01 % H_2O, VWR) was stored inside a glove box (MBraun Unilab, < 0.1 ppm H_2O, < 0.1 ppm O_2) under an argon atmosphere. All other solvents and reagents were of analytical grade or higher and were used without further purification.

2.2. Analytical methods

Attenuated total reflectance-Fourier transform infrared (ATR-FTIR)) spectra were recorded in the range of 4000–400 cm^{-1} on a Bruker Vector 22 spectrometer. Differential scanning calorimetry (DSC) thermograms were recorded using TA DSC Q200 (USA) with heating rates of 20 °C/min in nitrogen atmosphere. The samples were heated up to 250 °C and cooled down to the −60 °C at heating rate of 20 °C/min before the measurements. ^{1}H NMR spectra were recorded using a Bruker Ascend 400 NMR spectrometer (Germany) with a working frequency of 400 MHz. $CDCl_3$ was used as solvent in NMR experiments. Size exclusion chromatography (SEC) measurements were carried out in THF on a Tosoh Bioscience HLC- 8320GPC EcoSEC (Japan) system equipped with three PSS SDV columns of 5 μm (100 Å, 1000 Å, 100000 Å) (8 × 300 mm), as well as a UV and a differential refractive index detector. The operation temperature was set to 35 °C, with a flow rate of 1 mL min^{-1}. The system was calibrated using poly(methyl methacrylate) standards. Dynamic mechanical analysis (DMA) measurements were performed using an Eplexor 150 N Netsch dynamic mechanical analyzer (Germany) at a fixed frequency of 1 Hz using extension clamp. The samples having dimension of 30 mm × 8 mm × 0.1 mm were heated at a heating rate of 2 °C/min. Thermogravimetric analysis (TGA) was performed using TA TG5500 thermobalance (USA) at a heating rate of 10 °C min^{-1} up to 600 °C under nitrogen flow of 100 mL min^{-1}. X-ray diffraction (XRD) measurements of polymer films were conducted on a STADI-P (STOE) setup with Cu-$K_{\alpha1}$ radiation and transmission geometry. The measurements were performed in the 10-90° range, using a linear MYTHEN2 detector.

2.3. Synthesis of PI_{95}-PEO_5 copolymer

In a 10 mL two-neck round-shaped flask equipped with a magnetic stirrer and a nitrogen inlet/outlet 6FDA (0.45 g, 1.0129 mmol, 100 eq.) and Jeffamine ED-2003 (0.098 g, 0.0506 mmol, 5 eq.) were added together with 2.44 g of benzoic acid. The reaction mixture was stirred at 155 °C under flow of nitrogen. When all components become completely soluble, the mixture was stirred for 1 h. After that, HFBAPP (0.499 g, 0.9623 mmol, 95 eq.) was added to the reaction mixture and was stirred for additional 3 h. Then the hot reaction mixture was poured onto a Petri dish and cooled to room temperature. The solid reaction mass was ground in a mortar, and benzoic acid was extracted with ethanol. The product was dried under vacuum at 60 °C for 24 h. Yield: 77 %.

FT-IR (ATR, cm^{-1}): 2873 (C–H stretching of PEO), 1784 and 1720 (C=O symmetric and asymmetric vibration of imide cycle), 1374 and 745 (C—N bending of imide cycle), 1091 (C—O stretching of PEO), 828 (H—C–H rocking of PEO).

^{1}H NMR (400 MHz, $CDCl_3$) δ: 8.05 (d, J=8.0 Hz, Ar—H), 7.93 (s, Ar—H), 7.88 (d, J=7.9 Hz, Ar—H), 7.80 – 7.74 (m, Ar—H) 7.41 (e, J=9.3 Hz, Ar—H), 7.19 (d, J=8.9 Hz, Ar—H), 7.05 (d, J=8.9 Hz, Ar—H), 3.64 (s, C–H).

SEC (THF): M_n = 4.49 × 10^4 g/mol, M_w = 7.43 × 10^4 g/mol, $Đ$ = 1.65.

2.4. Synthesis of PI_{85}-PEO_{15} copolymer

In a 10 mL two-neck round-shaped flask equipped with a magnetic stirrer and a nitrogen inlet/outlet 6FDA (0.451 g, 1.0152 mmol, 100 eq.) and Jeffamine ED-2003 (0.2939 g, 0.1523 mmol, 15 eq.) were added together with 2.8 g of benzoic acid. The reaction mixture was stirred at 155 °C under flow of nitrogen. When all components become completely soluble, the mixture was stirred for 1 h. After that, HFBAPP (0.447 g, 0.8629 mmol, 85 eq.) was added to the reaction mixture and was stirred for additional 3 h. Then the hot reaction mixture was poured onto a Petri dish and cooled to room temperature. The solid reaction mass was ground in a mortar, and benzoic acid was extracted with ethanol. The product was dried under vacuum at 60 °C for 24 h. Yield: 77 %.

FT-IR (ATR, cm^{-1}): 2878 (C–H stretching of PEO), 1780 and 1720 (C=O symmetric and asymmetric vibration of imide cycle), 1378 and 746 (C—N bending of imide cycle), 1096 (C—O stretching of PEO), 829 (H—C–H rocking of PEO).

^{1}H NMR (400 MHz, $CDCl_3$) δ: 8.07 – 8.00 (m, Ar—H), 7.93 (s, Ar—H), 7.92 – 7.86 (m, Ar—H), 7.81 – 7.74 (m, Ar—H) 7.41 (t, J=9.2 Hz, Ar—H), 7.19 (d, J=8.0 Hz, Ar—H), 7.05 (d, J=8.4 Hz, Ar—H), 3.64 (s, C–H).

SEC (THF): $M_n = 2.89 \times 10^4$ g/mol, $M_w = 5.33 \times 10^4$ g/mol, $Đ$ = 1.84.

2.5. Synthesis of PI_{70}-PEO_{30} copolymer

In a 10 mL two-neck round-shaped flask equipped with a magnetic stirrer and a nitrogen inlet/outlet 6FDA (0.441 g, 0.9936 mmol, 100 eq.) and Jeffamine ED-2003 (0.575 g, 0.2981 mmol, 30 eq.) were added together with 2.8 g of benzoic acid. The reaction mixture was stirred at 155 °C under flow of nitrogen. When all components become completely soluble, the mixture was stirred for 1 h. After that, HFBAPP (0.361 g, 0.6955 mmol, 70 eq.) was added to the reaction mixture and was stirred for additional 3 h. Then the hot reaction mixture was poured onto a Petri dish and cooled to room temperature. The solid reaction mass was ground in a mortar, and benzoic acid was extracted with hot water. The product was dried under vacuum at 60 °C for 24 h. Yield: 78 %.

FT-IR (ATR, cm^{-1}): 2868 (C–H stretching of PEO), 1781 and 1716 (C=O symmetric and asymmetric vibration of imide cycle), 1377 and 747 (C—N bending of imide cycle), 1091 (C—O stretching of PEO), 830 (H—C–H rocking of PEO).

^{1}H NMR (400 MHz, $CDCl_3$) δ: 8.07 – 8.00 (m, Ar—H), 7.94 (s, Ar—H), 7.91 – 7.87 (m, Ar—H), 7.80 – 7.74 (m, Ar—H) 7.41 (t, J=9.5 Hz, Ar—H), 7.19 (d, J=8.4 Hz, Ar—H), 7.06 (d, J=8.4 Hz, Ar—H), 3.64 (s, C–H).

SEC (THF): $M_n = 2.87 \times 10^4$ g/mol, $M_w = 4.58 \times 10^4$ g/mol, $Đ$ = 1.59.

2.6. Positive electrode preparation and cycling of Li° | LFP polymer cell

For the preparation of positive electrodes for electrochemical tests 0.130 g of LFP, 0.040 g of carbon black, 0.010 g of PVdF, 0.010 g of LiTFSI, and 0.010 g of PI_{85}-PEO_{15} (65:20:5:5:5 ratio by mass) were weighed in a ball-mill container, and 1 mL of *N*-methyl-2-pyrrolidone was added. The container was transferred to a ball-mill mixer SPEX 8000, and the slurry was mixed for 10 min. Subsequently, the slurry was spread onto a conductive carbon-coated aluminum foil (MTI, 18 μm) using an automatic film applicator Zehntner ZAA 2300 with a gap width of 150 μm and dried after deposition at 60 °C. The mass loading was ~1.5 mg cm^{-2}. Round-shaped electrodes with a diameter of 14 mm were cut out and dried at 110 °C for 12 h under vacuum prior to use.

2.7. Preparation of solid polymer electrolyte

Prior to SPE preparation, the respective polymer was dried at 60 °C under vacuum for 24 h and introduced in to the glovebox. The polymer as well as the corresponding amount of LiTFSI salt with predefined ratios were both dissolved in anhydrous acetone. After complete dissolution, a homogenous mixture was casted into a Teflon dish. Acetone was removed slowly at room temperature overnight followed by additional drying of the polymer electrolyte film at 40 °C for 24 h in vacuum oven inside the glovebox. The resulting films with a thickness of ~200 μm were peeled off from the Teflon molds.

2.8. Electrochemical characterization

Electrochemical impedance spectroscopy (EIS) was measured using a coin-type cells (2032-type round button cell) that were assembled in an Ar-filled glovebox. Polymer films with a diameter of 10 mm were sandwiched between two stainless steel (SS) electrodes and measured using VSP potentiostat (BioLogic Science Instruments, France) over a frequency range from 1 MHz to 500 mHz with an amplitude of 20 mV. All samples were preconditioned overnight, in a temperature chamber Binder MK-56 (Germany) at 60 °C and then measured in temperature range between 20 and 70 °C with gradual temperature increase in 10 °C. Each temperature was held constant for 2 h before recording impedance spectra. Further, the bulk electrolyte resistance (R_b) was estimated from the Nyquist plot, and the ionic conductivity (σ) was calculated according to equation (1):

$$\sigma = \frac{1}{R_b}\frac{l}{A} \quad (1)$$

where l represents the thickness, and A represents the area of a SPE film.

Lithium-ion transference numbers (T_{Li}^+) were determined using the Bruce and Vincent method at 60 °C. Symmetric Li° /Li° cells were polarized at 10 mV until the current reached a steady-state to determine the initial current (I_0) and the steady-state current (I_{SS}). EIS was recorded before and after the polarization to get the initial interfacial resistance (R_0) and the steady state interfacial resistance (R_{SS}). T_{Li}^+ were calculated *via* the equation (2):

$$T_{Li^+} = \frac{I_{ss}(\Delta V - I_0 R_0)}{I_0(\Delta V - I_{ss}R_{ss})} \quad (2)$$

Linear sweep voltammetry (LSV) was conducted at 60 °C from OCV to 6 V for SS/SPE/Li° cell with a scanning rate of 1 mVs^{-1}. CR2032 cells (Li° | $LiFePO_4$) were assembled in an argon-filled glove box. The Li° | $LiFePO_4$ cells were charged and discharged in a potential range between 2.5 and 3.9 V at 60 °C.

A lithium plating-stripping test was performed for a Li°/SPE/Li° symmetrical cell with current densities of 0.01, 0.02, 0.05, and 0.1 mA cm^{-2} at 60 °C. During each cycle, the cell was charged/discharged for 1 h, followed by a 30-minute rest period.

3. Results and discussion

3.1. Synthesis and characterization of the copolymers

A series of PI-PEO copolymers were synthesized using one-pot, two step synthesis in benzoic acid melt (Scheme 1) [65,66]. Using of benzoic acid as an active media allows the synthesis of high molecular weight PI-PEO copolymers without using toxic solvents, such as *N*-methyl-2-pyrrolidon [60,61] or dimethylacetamide [50,62]. Benzoic acid catalyzes the imidization reaction and no additional treatment is needed, in contrast to the traditional two-stage method. Copolymers PI_{95}-PEO_5, PI_{85}-PEO_{15} and PI_{70}-PEO_{30} were synthesized with different mole ratios, as described in experimental section. In accordance with the molar ratio between Jeffamine ED-2003 and HFBAPP, copolymers were designated as PI_{95}-PEO_5, PI_{85}-PEO_{15} and PI_{70}-PEO_{30}, respectively. Syntheses of copolymers were performed in two steps: in the first step a predefined amount of Jeffamine ED-2003 reacted with an excess of 6FDA leading to oligomers with anhydride end groups. In the second step, aromatic diamine HFBAPP was introduced up to equimolar concentration between amine and anhydride groups. For polymers PI_{95}-PEO_5 and PI_{85}-PEO_{15}, benzoic acid was extracted using ethanol. Because PI_{70}-PEO_{30} swelled in ethanol, it was purified with hot water.

The chemical structures of the copolymers were characterized using ^{1}H NMR. Fig. 1 illustrates the ^{1}H NMR spectrum of PI_{95}-PEO_5, which is representative for all polymers. Model compounds (diimides) based on 6FDA, 4,4′-(4,4′-isopropylidenediphenoxy)diphthalic anhydride and 4-aminophenyl propargyl ether were previously described in literature, and their NMR spectra were used for correct assignments [67]. The signals observed at 8.06–8.04 ppm (1), 7.94 ppm (2) and 7.90–7.88 ppm (3) were assigned to the aromatic protons coupled with imide ring in 6FDA. The proton signals originating from HFBAPP appeared at

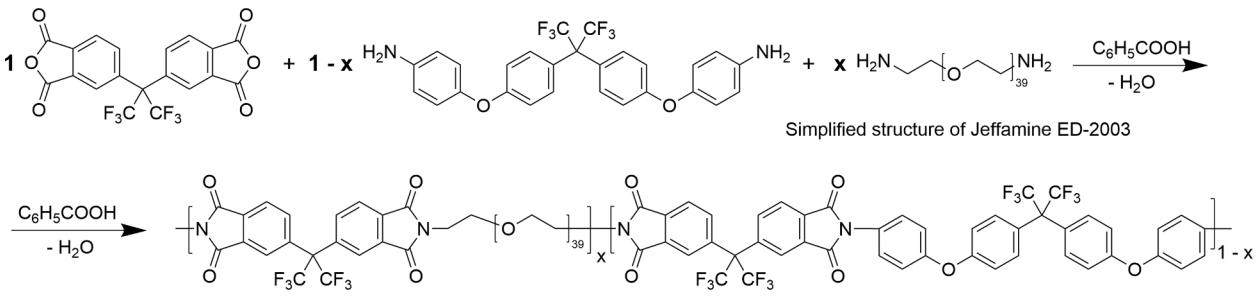

Scheme 1. Synthetic routes for PI-PEO copolymers (x = 0.05; 0.15; 0.3).

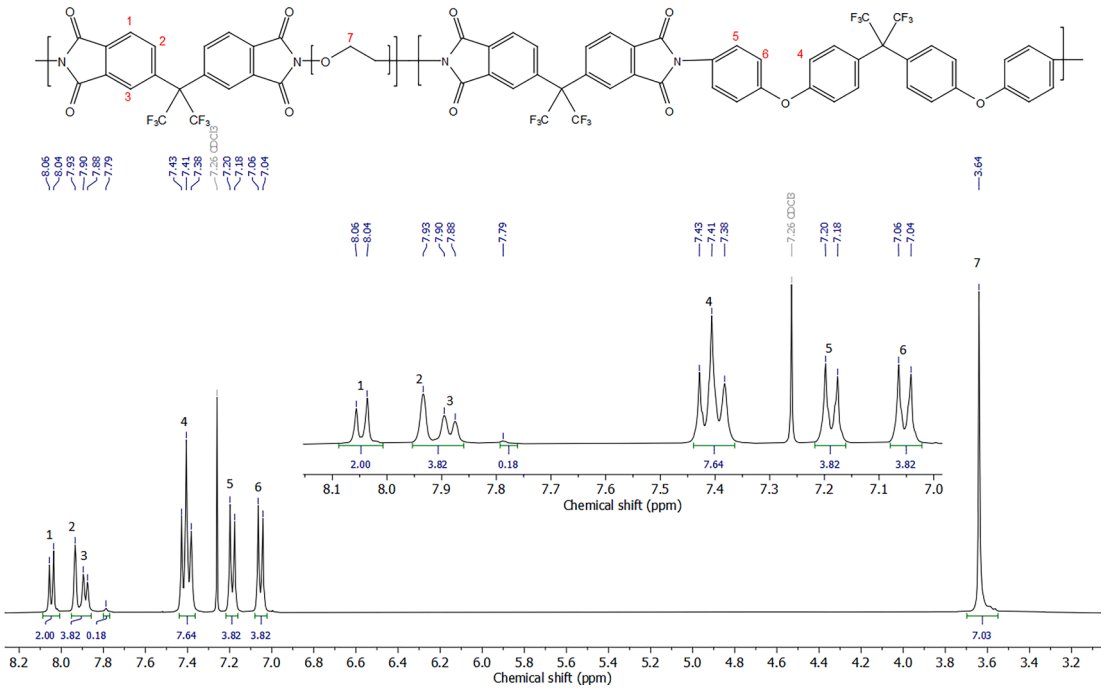

Fig. 1. ^{1}H NMR spectrum of PI_{95}-PEO_5 copolymer.

7.43–7.38 ppm (4,5), 7.21–7.18 ppm (6) and 7.07–7.04 ppm (7). The alkyl protons of Jeffamine were identified in the high field at 3.64 ppm (8). From the integration results, experimental molar block ratios were calculated based on the ratio between aliphatic and aromatic protons. Additionally, experimental ratios of PEO:HFBAPP are summarized in Table 1. The chemical structures of PI_{85}-PEO_{15} and PI_{70}-PEO_{30} were also confirmed *via* ^{1}H NMR spectroscopy, and the comparative spectra are presented in the Supplementary Information (Figures S1 – S3). An increase in the concentration of PEO blocks led to the appearance of new signals in the aromatic region at 8.02–8.00 ppm, 7.90–7.88 ppm and 7.80–7.75 ppm. These signals were attributed to the 6FDA fragment linked with the aliphatic diamine. Furthermore, the fraction of detected aromatic protons in the copolymers decreased in comparison to the fraction of aliphatic protons of PEO, when increasing the feed ratio between Jeffamine ED-2003 and HFBAPP. Additionally, for the correct assignment, COSY spectrum of PI_{85}-PEO_{15} are shown in the Supplementary Information (Figure S4).

The ATR-FTIR spectra of copolymers are shown in the Supplementary Information (Figures S5 – S7). All polymers show the absorption bands at 1780 cm^{-1} (symmetric imide C=O stretching), 1720 cm^{-1} (asymmetric imide C=O stretching) as well as at 1375 cm^{-1} and 745 cm^{-1}, corresponding to C—N stretching of the imide ring, confirming

Table 1
Targeted and experimental blocks ratio of the PI-PEO copolymers.

Sample	Feed mole ratio of HFBAPP:PEO	Observed molar ratio of HFBAPP:PEO by ^{1}H NMR	Target wt. % of PEO fraction	Experimental wt. % of PEO fraction from ^{1}H NMR (%)	Experimental wt. % of PEO fraction from TGA (%)	$T_{5\%}$[1] (°C)	C^{2}_{600} (%)
PI_{95}-PEO_5,	0.95:0.05	0.955:0.045	9.3	8.5	9.5	375	55
PI_{85}-PEO_{15}	0.85:0.15	0.863:0.137	24.6	22.9	23.5	355	39
PI_{70}-PEO_{30}	0.7:0.30	0.721:0.279	41.8	39.7	41.1	345	28

[1] Temperature of 5% weight loss in nitrogen atmosphere.
C^{2}_{600} char yields at 600 °C.

successful imidization. The characteristic peak at 2870 cm^{-1} due to the stretching of C–H, at 1090 cm^{-1} due to the stretching of C—O, and at 830 cm^{-1} due to the rocking vibrations of H—C–H increased with the higher PEO content. Overall, the FTIR and NMR spectra demonstrated good alignment with previously reported PI-PEO copolymers [60].

Generally, polyimides have a low solubility in common organic solvents due to strong interchain interactions and their rigid structure [40]. However, the presence of long aliphatic chain of PEO and bulky fluorinated substituent significantly increased the solubility of PI-PEO copolymers. All polymers were soluble in common organic solvents, such as *N,N*-dimethylformamide (DMF), *N*-methylpyrrolidone (NMP), tetrahydrofuran (THF), acetonitrile and toluene. The copolymer PI_{70}-PEO_{30}, with highest concentration of PEO content, was even soluble in ethanol and *n*-hexane. This enhanced solubility of PI-PEO copolymers enabled a thorough SEC characterization. The results of the SEC measurements and the solubility of copolymers are summarized in Table 2. All copolymers exhibited low dispersities ($Đ < 2.0$), considering the polymers were obtained by polycondensation. The copolymer with the highest concentration of HFBAPP demonstrated the highest molecular weight, likely due to its higher reactivity and purity compared to Jeffamine. SEC curves of copolymers are presented in the Supplementary Information (Figure S8). The obtained values of molecular weight were close to those previously reported for polyimides that were used for lithium metal batteries [56,57].

3.2. Thermal properties of the copolymers

All copolymers were also analyzed *via* DSC using a heating rate of 20 °C min^{-1} and the resulting thermograms are presented in Fig. 2. An amorphous structure is crucial for polymer electrolytes as there typically no ion transport is observed in crystalline regions [24,68]. All copolymers exhibited an amorphous nature as evidenced by the absence of endothermic peaks corresponding to melting, i.e., DSC curves showed the clear absence of PEO melting peaks. The presence of bulky fluorinated substituents and interchain interactions between imide rings likely inhibited crystallization of PEO. The temperature of the glass transition shifted depending on the ratio between aliphatic and aromatic blocks. PI_{70}-PEO_{30} exhibited the lowest glass transition temperature at 24 °C due to the highest fraction of PEO. As the aromatic polyimide block content increased, glass transition temperature rose, reaching 96 °C and 195 °C for PI_{85}-PEO_{15} and PI_{95}-PEO_5, respectively. Therefore, by adjusting the ratio between the aromatic PI block and the aliphatic PEO block, the glass transition temperature of the copolymers can be tuned. The amorphous structures of the copolymers were further confirmed by X-ray diffraction (Figure S9). As can be seen from the diffractograms, all samples demonstrate a broad amorphous halo without any distinguishable reflections. In contrast to the polydimethylsiloxane-polyimide copolymers, the copolymers synthesized in this work do not exhibit phase separation [69].

Thermal stability of copolymers was evaluated using TGA in nitrogen atmosphere. Good thermal stability is of great importance for polymer electrolytes [11]. TGA measurements were performed in a range from 50 °C to 600 °C at a heating rate of 10 °C min^{-1}. TGA curves of copolymers are shown in Fig. 3. It is widely acknowledged that fluorinated polyimides possess better thermal stability due to the higher bond strength of C—F [67,70], which is reflected in the TGA curves. The

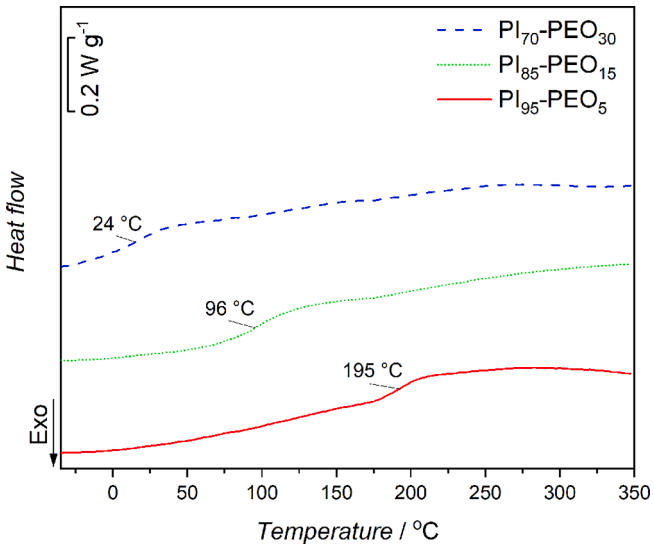

Fig. 2. DSC thermograms of PI-PEO copolymers.

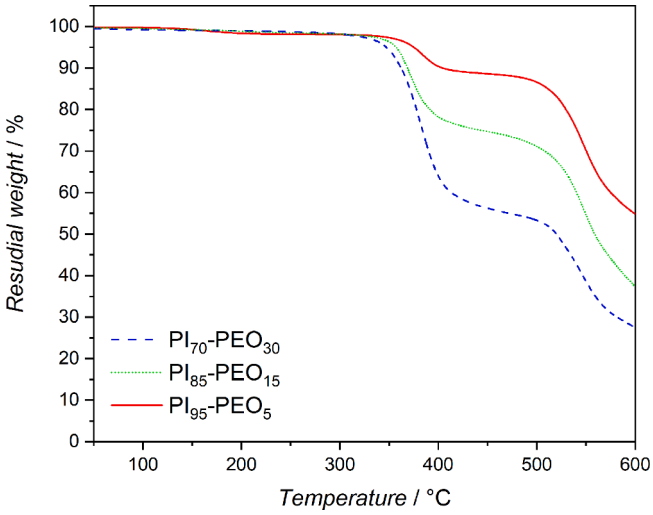

Fig. 3. TGA curves of PI-PEO copolymers in nitrogen.

thermal decomposition of PI-PEO copolymers occurred in two steps. Initially, a degradation of less thermally stable, aliphatic chain took place between 310 °C and 410 °C. Subsequently, at the higher temperatures, decomposition of aromatic block took place. The distinct separation of these two decomposition stages allowed for the additional evaluation of the content of the PEO fraction by the end of the first degradation step. The residual weight fraction of the copolymers after the first decomposition step, as well as the temperatures of 5 % weight loss, are summarized in Table 1. The values obtained from TGA are consistent with those from NMR spectroscopy, confirming the successful synthesis of copolymers with a block ratio close to the targeted one. Temperature of 5 % weight loss as well as char yields at 700 °C increased

Table 2
Targeted and experimental blocks ratio of the copolymers.

Sample	Solvent									M_n (g/mol)	M_w (g/mol)	$Đ$
	NMP	DMF	THF	$CHCl_3$	ACN	Acetone	$(C_2H_5)_2O$	C_2H_5OH	C_6H_{14}	$\times 10^4$	$\times 10^4$	$Đ$
PI_{95}-PEO_5,	+	+	+	+	–	+	+	–	–	4.49	7.43	1.65
PI_{85}-PEO_{15}	+	+	+	+	+	+	+	–	–	2.89	5.33	1.84
PI_{70}-PEO_{30}	+	+	+	+	+	+	+	+	+	2.87	4.58	1.59

+ soluble, – insoluble.

with an increase in the HFBAPP:PEO mole ratio due to a decrease in the less thermally stable PEO fraction. All copolymers exhibited excellent thermal stabilities and could be utilized at high temperatures, up to 350 °C.

As SPEs serve the dual role of separator and electrolyte, possessing good mechanical properties is crucial for suppressing dendrite formation and preventing short-circuits [71,72]. All prepared copolymers showed good film-forming properties after casting from solution, yielding self-standing films of ~ 100 μm at room temperature. To evaluate the mechanical properties of films at different temperatures, DMA was used. The plots of the storage modulus as a function of temperature are shown in Fig. 4. Copolymer PI_{95}-PEO_5 and PI_{85}-PEO_{15} showed good mechanical properties with a modulus exceeding 2 GPa up to their glass transition. However, at temperatures of 82 °C and 178 °C for PI_{85}-PEO_{15} and PI_{95}-PEO_5, respectively, a significant decrease in storage modulus occurred, corresponding to the transition from the glassy state to the rubbery state. Due to its low glass transition temperature, copolymer PI_{70}-PEO_{30} experienced a decrease in storage modulus at lower temperatures, reaching a value of 400 MPa at 25 °C. Therefore, only copolymers PI_{95}-PEO_5 and PI_{85}-PEO_{15} were further considered for application as polymer electrolytes.

3.3. Properties of polymer electrolytes

The polymer electrolytes based on the PI-PEO copolymers were prepared using solution casting technique. First, the feasibility of preparation homogenous solutions of the copolymers with LiTFSI in acetone was investigated. The presence of PEO chains in the copolymers, enabled the coordination of lithium salt, facilitating the dissolution LiTFSI in high concentration to form a polymer-in-salt electrolyte (with concentration of LiTFSI>50 wt%) [73,74]. Noteworthy, PI_{95}-PEO_5 featuring the lowest concentration of PEO, could only dissolve up to 40 wt% of LiTFSI. Consequently, PEO primarily facilitated the dissolution of LiTFSI, while the PI block enhanced the mechanical properties. For an objective comparison, compositions with 40 wt% of LiTFSI were prepared for all copolymers, and their ionic conductivities were measured from 20 °C to 70 °C, as depicted in Fig. 5a. After the preparation of SPE, the glass transition temperature cannot be measured using DSC due to the high salt content. This is a common feature of compositions with high salt content, especially for polymer-in-salt compositions [3].

All copolymers demonstrated a gradual increase in conductivity with increasing temperature. As observed from the Arrhenius plot, at a concentration of 40 wt% of LiTFSI, all copolymers exhibited ionic conductivities in the same order of magnitude. The increase in the fluorinated imide block decreases the dependence of ionic conductivity on temperature. This effect may arise from different ethylene oxide/lithium ratios or from the enhanced chain mobility of copolymers with higher PEO concentrations. However, PEO blocks are responsible for the dissolution of lithium salt, which is why the PI_{95}-PEO_5 copolymer was unable to dissolve a higher amount of LiTFSI than 40 wt% due to the low fraction of PEO chains.

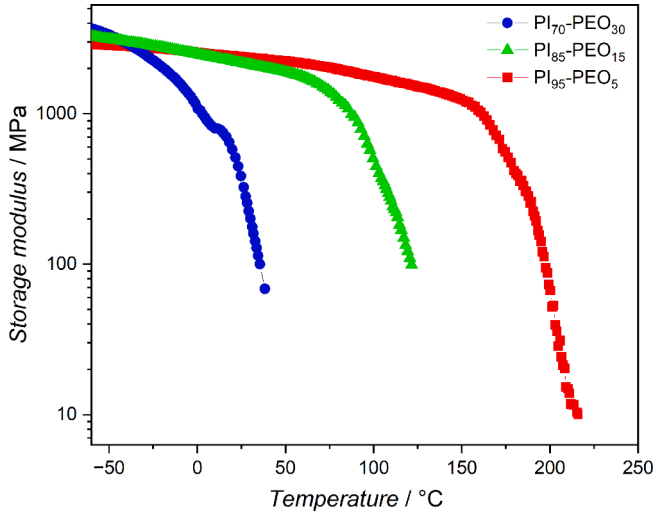

Fig. 4. Dependence of storage modulus from temperature for copolymers measured by DMA.

Therefore, PI_{85}-PEO_{15} copolymer was utilized to investigate the influence of salt concentration on the ionic conductivity. The dependence of ionic conductivity on temperature for PI_{85}-PEO_{15} with different LiTFSI concentrations was measured using EIS. Ionic conductivity was measured from 20 °C to 70 °C, and the results are depicted in Fig. 5b. It was observed, that with an increase in salt concentration from 40 wt%, up to 70 wt%, the ionic conductivity gradually increased. Specifically, the ionic conductivity of PI_{85}-PEO_{15} increased from 1.2×10^{-6} S cm^{-1} for composition with 40 wt% up to 1.34×10^{-4} S cm^{-1} for composition with 70 wt% at 70 °C. A similar trend of increasing ionic conductivity with increase of salt content was shown in work of J. Zhang *et al.* when a "polymer in salt" level was reached [75]. With an increase in salt content, the free volume in the polymer electrolyte also rises, leading to higher charge carrier mobility between anion clusters, and an increase in ionic conductivity [76]. Additionally, the presence of specific Li–anion–polycation co-coordination has been previously demonstrated for poly(ionic liquid)s, showing increased ionic conductivity with an increase in salt concentrations using molecular dynamics simulation [77,78]. Therefore, the presence of charge transfer complex in polyimides, formed between alternating electron-donor (diamine) and electron-acceptor (dianhydride) moieties [41,79] might contribute to such an ionic conductivity behavior. Therefore, we assume the ion-hopping mechanism is predominant in this system, which is common for high concentrated polymer electrolytes [80]. All compositions exhibited a nonlinear growth in ionic conductivity as the temperature increased, corresponding to a water-free polymer electrolyte [76]. The conductivity plot demonstrated gradual increase of ionic conductivity with rise of temperature in the 20 °C to 70 °C region. For composition containing 70 wt% of LiTFSI, the ionic conductivity rose from 1.21×10^{-6} S cm^{-1} at 20 °C to 1.34×10^{-4} S cm^{-1} at 70 °C.

The copolymer PI_{85}-PEO_{15} with 70 wt% of LiTFSI was selected for further experiments as it showed the highest ionic conductivity among the tested series. To estimate lithium-ion transference numbers (T_{Li}^{+}) the Bruce-Vincent method was employed [81]. The chronoamperometry profile of the symmetric cell and the Nyquist plots before and after polarization at 60 °C are presented in Supplementary Information, Figure S10. It is known that polymer-salt compositions exhibit a steep increase in the T_{Li}^{+} with an increasing amount of salt [82]. The molar ratio between ethylene oxide repeating units and Li^{+} for the copolymer PI_{85}-PEO_{15} with 70 wt% of LiTFSI was 0.7:1. Thus, T_{Li}^{+} was calculated to be 0.7, which is common for polymer-in-salt compositions with high salt concentration [74,78,83]. Additionally, it was previously reported that fluorine-containing blocks interact strongly with the anion of LiTFSI and limit its movability, leading to an increased T_{Li}^{+} [84,85]. Further, the electrochemical stability of copolymer PI_{85}-PEO_{15} with 70 wt% of LiTFSI was investigated using LSV. As shown in Figure S11 in Supplementary Information the electrolyte demonstrated a two-step oxidation with a minor oxidation peak at a potential higher than 4 V *vs.* Li/Li^{+}. This minor oxidation process could be attributed to the gradual oxidation of aliphatic PEO chains of the copolymer. A similar observation, with a two-step degradation, was demonstrated by Aldalur *et al.* for poly (ethylene-*alt*-maleic anhydride) with grafted Jeffamine side chains [86] and for polybenzoxazine-PEO copolymers [38].

To demonstrate the enhancement in flame-retardant properties of PI-PEO based electrolytes, a combustion test was conducted. As shown in the Supplementary Information (Video-1), the polymer film PI_{85}-PEO_{15} with 70 wt% of LiTFSI, was exposed to a flame for 5 s, but did not ignite and demonstrated an outstanding self-extinguishing behavior.

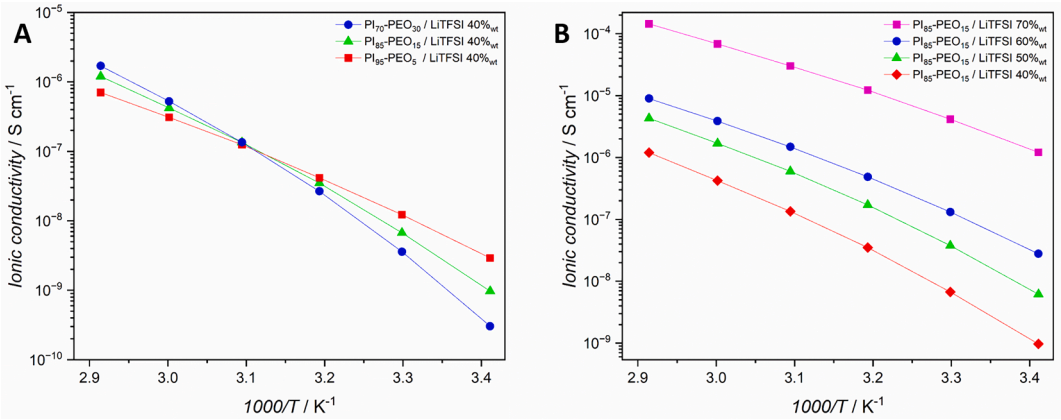

Fig. 5. (a) Temperature dependence of ionic conductivity of PI_{95}-PEO_5, PI_{85}-PEO_{15} and PI_{70}-PEO_{30} with 40 % salt concentration, (b) temperature dependence of ionic conductivity of PI_{85}-PEO_{15} with different salt concentration.

Conversely, polymer electrolytes based on PEO with 20:1 EO/Li ratio of LiTFSI ignited upon contact with fire immediately and burned out (Video-2). Results of flame tests are summarized in Fig. 6. The non-flammable properties of the PI_{85}-PEO_{15} polymer electrolyte may be attributed to the high concentration of inorganic salt and the presence of a trifluoromethyl group in the PI backbone, which provided excellent flame retardancy [87,88].

To probe interface stability between PI-PEO copolymer and lithium metal, plating/stripping test was performed at different current densities. A symmetric Li°/PI_{85}-PEO_{15}-LiTFSI 70 wt%/Li cell was assembled and investigated at 60 °C. The cell was cycled with gradually increasing current densities of 0.01, 0.02, 0.05, and 0.1 mA cm^{-2}, alternating between charge/discharge and relaxation steps. As seen in Figure S12, the symmetrical Li-cell demonstrated reversible metal deposition at current densities from 0.01 up to 0.1 mA cm^{-2}. At current densities of 0.01, 0.02, and 0.05 mA cm^{-2} the cell exhibited stable overpotentials of ~ 30, 60, and 200 mV, respectively. However, at current densities of 0.1 mA cm^{-2}, a dramatic increase in overpotential was observed, reaching the limiting cut-off of 2 V, and overpotential became unstable during the application of positive and negative current. Overall the experiments with the PI-PEO copolymer suggest good interface compatibility with lithium metal. Lastly, the electrochemical performance in terms of capacity retention and cycle life of PI_{85}-PEO_{15} with 70 wt% of LiTFSI was evaluated in a LMB, using LFP as positive electrode. A small fraction of copolymer was introduced into the electrode to improve interphase contact with the electrolyte. The loading of active material was 1.5 mg/cm^2. The cell was cycled at 0.1C for 50 cycles at 60 °C. Initially, issues were encountered during the construction of the cells due to insufficient infiltration of SPE into the porous LFP cathode leading to the low discharge capacity (<100 mAh/g). Similar issues were noted for polyurethane-polycarbonate copolymers [89]. This resulted in a large portion of the LFP being inaccessible for Li^+ transport, leading to low capacities and ultimately to cell failure. Therefore, it is necessary to include SPE in the electrode formulation to enable sufficient contact between SPE and active material. The loading of active material was 1.5 mg/cm^2. The cell was cycled at 0.1C for 50 cycles. Fig. 7a illustrates the cycling performance of the battery with PI_{85}-PEO_{15}-70 wt%. The cell demonstrated a discharge capacity of 152 mAh/g during the first cycle, which is close to the theoretical value of 170 mAh/g, along with high coulombic efficiency (98.3 %). Overall, the cell maintained high columbic efficiency during 50 cycles with a capacity retention of 81.4 % after 50 cycles. The capacity decay may be attributed to side reactions on the electrode surface [90]. Fig. 7b shows smooth charge–discharge curves without noticeable noise, indicating the prevention of soft dendrite growth likely due to the good mechanical properties of the SPE.

4. Conclusions

In this study, non-flammable polyimide-poly(ethylene oxide) copolymers were successfully synthesized using a facile, eco-friendly method in a benzoic acid melt and utilized as polymer electrolyte for lithium metal batteries. Copolymers with molar ratios of 5:95, 15:85 and 30:70 between PEO and aromatic diamine were synthesized. Chemical structures of copolymers were confirmed *via* ^1H NMR and IR-spectroscopy. An increase in the PEO:PI block ratio led to a decrease in glass transition temperature and thermal stability, accompanied by

Fig. 6. Results of flame tests of PEO with 20:1 EO/Li ratio of LiTFSI (top) and PI_{85}-PEO_{15} with 70 wt% LiTFSI (bottom).

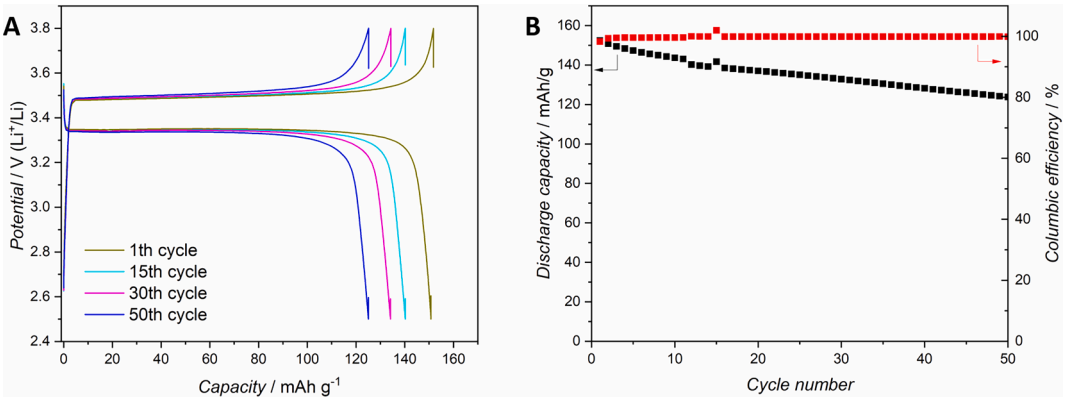

Fig. 7. Charge-discharge curves (a) and the cycling performance of $LiFePO_4$/ PI_{85}-PEO_{15}-LiTFSI 70 wt%/Li cell at 60 °C at the current density of 0.1C (b).

improved solubility in organic solvents, demonstrating the possibility of precise control of polymer properties. All copolymers exhibited amorphous structure and demonstrated high thermal stability with two step decomposition. Copolymers PI_{85}-PEO_{15} and PI_{95}-PEO_5 displayed excellent mechanical properties according to DMA studies, rendering them suitable for application as polymer electrolytes. PI_{85}-PEO_{15} copolymer was capable of dissolving up to 70 wt% of LiTFSI, achieving a polymer-salt composition, while PI_{95}-PEO_5 dissolved only 40 wt%. The increase in conductive salt concentration led to a gradual rise in ionic conductivity, reaching 1.34×10^{-4} S cm^{-1} at 70 °C. Polymer-in-salt composition and charge transfer complex contributed to a high transference number, as measured by the Bruce-Vincent method. In addition, the polymer electrolyte exhibited non-flammable properties, as demonstrated by combustion tests. Lastly, the LMB with LFP displayed promising electrochemical performance, including a high initial discharge capacity of 152 mAh/g, high columbic efficiency, and a capacity retention of 81.4 % after 50 cycles at 0.1C that is comparable with other SPE for high temperature application [89,91,92]. This study introduces a tunable polymer system for the fabrication of non-flammable, high-performing, and safe polymer electrolytes for LMB, thereby opening avenues for further research in this field.

CRediT authorship contribution statement

Timofey I. Kolesnikov: Writing – original draft, Investigation, Data curation. **Dominik Voll:** Writing – review & editing. **Fabian Jeschull:** Writing – review & editing, Supervision, Conceptualization. **Patrick Theato:** Writing – review & editing, Supervision, Conceptualization.

Declaration of competing interest

The authors declare that they have no known competing financial interests or personal relationships that could have appeared to influence the work reported in this paper.

Data availability

The data that support the findings of this study are openly available in www.radar-service.eu at 10.22000/jGCCRAkGwdLQxdIQ.

The data that support the findings of this study are openly available in https://www.radar-service.eu at https://doi.org/10.22000/jGCCRAkGwdLQxdIQ.

Acknowledgements

This work contributes to the research performed at CELEST (Center for Electrochemical Energy Storage Ulm-Karlsruhe) and was funded by the German Research Foundation (DFG) under Project ID 390874152 (POLiS Cluster of Excellence), as well as DFG grant #448719339. The authors would like to thank Daniel Zimmermann for help with DMA and Dr. Arseniy Bokov for XRD measurements.

Appendix A. Supplementary material

Supplementary data to this article can be found online at https://doi.org/10.1016/j.eurpolymj.2024.113315.

References

[1] G.E. Blomgren, The development and future of lithium ion batteries, J. Electrochem. Soc. 164 (2017) A5019–A5025, https://doi.org/10.1149/2.0251701jes.
[2] Y. Chen, Y. Kang, Y. Zhao, L. Wang, J. Liu, Y. Li, Z. Liang, X. He, X. Li, N. Tavajohi, B. Li, A review of lithium-ion battery safety concerns: The issues, strategies, and testing standards, J. Energy Chem. 59 (2021) 83–99, https://doi.org/10.1016/j.jechem.2020.10.017.
[3] D.Y. Voropaeva, S.A. Novikova, A.B. Yaroslavtsev, Polymer electrolytes for metal-ion batteries, Russ. Chem. Rev. 89 (2020) 1132–1155, https://doi.org/10.1070/RCR4956.
[4] L. Long, S. Wang, M. Xiao, Y. Meng, Polymer electrolytes for lithium polymer batteries, J. Mater. Chem. A. 4 (2016) 10038–10069, https://doi.org/10.1039/C6TA02621D.
[5] L. Yue, J. Ma, J. Zhang, J. Zhao, S. Dong, Z. Liu, G. Cui, L. Chen, All solid-state polymer electrolytes for high-performance lithium ion batteries, Energy Storage Mater. 5 (2016) 139–164, https://doi.org/10.1016/j.ensm.2016.07.003.
[6] J. Chen, L. Rong, X. Liu, J. Liu, S. Peng, X. Jiang, Flame retardant polyurethane acrylate solid polymer electrolyte based on the synergistic effect of modified halloysite nanotubes for safe lithium batteries, Eur. Polym. J. 194 (2023) 112190, https://doi.org/10.1016/j.eurpolymj.2023.112190.
[7] G. Rollo-Walker, J. White, J. Chiefari, M. Forsyth, N. Malic, 'One-pot' RAFT polymerization and characterization of quasi-block copolymers; a comparison to traditional block copolymer for use as solid polymer electrolytes, Eur. Polym. J. 199 (2023) 112450, https://doi.org/10.1016/j.eurpolymj.2023.112450.
[8] D. Voropaeva, S. Novikova, N. Trofimenko, A. Yaroslavtsev, Polystyrene-based single-ion conducting polymer electrolyte for lithium metal batteries, Processes. 10 (2022) 2509, https://doi.org/10.3390/pr10122509.
[9] X. Zeng, M. Li, D. Abd El-Hady, W. Alshitari, A.S. Al-Bogami, J. Lu, K. Amine, Commercialization of lithium battery technologies for electric vehicles, Adv. Energy Mater. 9 (2019), https://doi.org/10.1002/aenm.201900161.
[10] X.-B. Cheng, R. Zhang, C.-Z. Zhao, Q. Zhang, Toward Safe lithium metal anode in rechargeable batteries: a review, Chem. Rev. 117 (2017) 10403–10473, https://doi.org/10.1021/acs.chemrev.7b00115.
[11] M. Chen, Z. Yue, Y. Wu, Y. Wang, Y. Li, Z. Chen, Thermal stable polymer-based solid electrolytes: design strategies and corresponding stable mechanisms for solid-state Li metal batteries, Sustain. Mater. Technol. 36 (2023) e00587, https://doi.org/10.1016/j.susmat.2023.e00587.
[12] D. Zhou, D. Shanmukaraj, A. Tkacheva, M. Armand, G. Wang, Polymer Electrolytes for lithium-based batteries: advances and prospects, Chem. 5 (2019) 2326–2352, https://doi.org/10.1016/j.chempr.2019.05.009.
[13] J. Mindemark, M.J. Lacey, T. Bowden, D. Brandell, Beyond PEO—Alternative host materials for Li + -conducting solid polymer electrolytes, Prog. Polym. Sci. 81 (2018) 114–143, https://doi.org/10.1016/j.progpolymsci.2017.12.004.
[14] Z. Xue, D. He, X. Xie, Poly(ethylene oxide)-based electrolytes for lithium-ion batteries, J. Mater. Chem. A. 3 (2015) 19218–19253, https://doi.org/10.1039/C5TA03471J.
[15] G. Rollo-Walker, N. Malic, X. Wang, J. Chiefari, M. Forsyth, Development and progression of polymer electrolytes for batteries: influence of structure and

chemistry, Polymers (Basel). 13 (2021) 4127, https://doi.org/10.3390/polym13234127.
[16] P.V. Wright, Electrical conductivity in ionic complexes of poly(ethylene oxide), Br. Polym. J. 7 (1975) 319–327, https://doi.org/10.1002/pi.4980070505.
[17] D.E. Fenton, J.M. Parker, P.V. Wright, Complexes of alkali metal ions with poly (ethylene oxide), Polymer (Guildf). 14 (1973) 589, https://doi.org/10.1016/0032-3861(73)90146-8.
[18] M.B. Armand, Polymer electrolytes, Annu. Rev. Mater. Sci. 16 (1986) 245–261, https://doi.org/10.1146/annurev.ms.16.080186.001333.
[19] X. Judez, G.G. Eshetu, C. Li, L.M. Rodriguez-Martinez, H. Zhang, M. Armand, Opportunities for rechargeable solid-state batteries based on Li-intercalation cathodes, Joule. 2 (2018) 2208–2224, https://doi.org/10.1016/j.joule.2018.09.008.
[20] W. Sun, C. Ma, F. Dong, X. Zhang, Y. Sun, K. Chen, H. Xie, J. Liu, Poly(lactic acid) block improves ambient-temperature ionic conductivity of pentablock copolymer electrolyte, J. Power Sources. 591 (2024) 233901, https://doi.org/10.1016/j.jpowsour.2023.233901.
[21] C. Xue, M.A.B. Meador, L. Zhu, J.J. Ge, S.Z.D. Cheng, S. Putthanarat, R.K. Eby, A. Khalfan, G.D. Bennett, S.G. Greenbaum, Morphology of PI–PEO block copolymers for lithium batteries, Polymer (Guildf). 47 (2006) 6149–6155, https://doi.org/10.1016/j.polymer.2006.06.024.
[22] J.L. Olmedo-Martínez, L. Porcarelli, G. Guzmán-González, I. Calafel, M. Forsyth, D. Mecerreyes, A.J. Müller, Ternary poly(ethylene oxide)/poly(l, l-lactide) PEO/PLA blends as high-temperature solid polymer electrolytes for lithium batteries, ACS Appl. Polym. Mater. 3 (2021) 6326–6337, https://doi.org/10.1021/acsapm.1c01093.
[23] J.L. Olmedo-Martínez, L. Porcarelli, Á. Alegría, D. Mecerreyes, A.J. Müller, High lithium conductivity of miscible poly(ethylene oxide)/methacrylic sulfonamide anionic polyelectrolyte polymer blends, Macromolecules. 53 (2020) 4442–4453, https://doi.org/10.1021/acs.macromol.0c00703.
[24] L. Zhu, J. Li, Y. Jia, P. Zhu, M. Jing, S. Yao, X. Shen, S. Li, F. Tu, Toward high performance solid-state lithium-ion battery with a promising <scp>PEO</scp> / <scp>PPC</scp> blend solid polymer electrolyte, Int. J. Energy Res. 44 (2020) 10168–10178, https://doi.org/10.1002/er.5632.
[25] C. Piedrahita, V. Kusuma, H.B. Nulwala, T. Kyu, Highly conductive, flexible polymer electrolyte membrane based on poly(ethylene glycol) diacrylate-co-thiosiloxane network, Solid State Ionics. 322 (2018) 61–68, https://doi.org/10.1016/j.ssi.2018.05.006.
[26] B. Chen, Q. Xu, Z. Huang, Y. Zhao, S. Chen, X. Xu, One-pot preparation of new copolymer electrolytes with tunable network structure for all-solid-state lithium battery, J. Power Sources. 331 (2016) 322–331, https://doi.org/10.1016/j.jpowsour.2016.09.063.
[27] C. Xin, K. Wen, S. Guan, C. Xue, X. Wu, L. Li, C.-W. Nan, A cross-linked poly (ethylene oxide)-based electrolyte for all-solid-state lithium metal batteries with long cycling Stability, Front. Mater. 9 (2022), https://doi.org/10.3389/fmats.2022.864478.
[28] J.S. Moreno, M. Armand, M.B. Berman, S.G. Greenbaum, B. Scrosati, S. Panero, Composite PEOn:NaTFSI polymer electrolyte: Preparation, thermal and electrochemical characterization, J. Power Sources. 248 (2014) 695–702, https://doi.org/10.1016/j.jpowsour.2013.09.137.
[29] W. Wieczorek, Z. Florjanczyk, J.R. Stevens, Composite polyether based solid electrolytes, Electrochim. Acta. 40 (1995) 2251–2258, https://doi.org/10.1016/0013-4686(95)00172-B.
[30] A.D. Khudyshkina, U. Rauska, A.J. Butzelaar, M. Hoffmann, M. Wilhelm, P. Theato, F. Jeschull, Impact of nano-sized inorganic fillers on PEO-based electrolytes for potassium batteries, Batter. Supercaps. 7 (2024), https://doi.org/10.1002/batt.202300404.
[31] X. Zhang, Y. Sun, C. Ma, N. Guo, H. Fan, J. Liu, H. Xie, Li6.4La3Zr1.4Ta0.6O12 reinforced polystyrene-Poly(ethylene oxide)-Poly(propylene oxide)-Poly(ethylene oxide)-polystyrene pentablock copolymer-based composite solid electrolytes for solid-state lithium metal batteries, J. Power Sources. 542 (2022) 231797, https://doi.org/10.1016/j.jpowsour.2022.231797.
[32] R. Bouchet, T.N.T. Phan, E. Beaudoin, D. Devaux, P. Davidson, D. Bertin, R. Denoyel, Charge transport in nanostructured PS–PEO–PS triblock copolymer electrolytes, Macromolecules. 47 (2014) 2659–2665, https://doi.org/10.1021/ma500420w.
[33] A.J. Butzelaar, P. Röring, T.P. Mach, M. Hoffmann, F. Jeschull, M. Wilhelm, M. Winter, G. Brunklaus, P. Théato, Styrene-based poly(ethylene oxide) side-chain block copolymers as solid polymer electrolytes for high-voltage lithium-metal batteries, ACS Appl. Mater. Interfaces. 13 (2021) 39257–39270, https://doi.org/10.1021/acsami.1c08841.
[34] F. Yuan, H.-Z. Chen, H.-Y. Yang, H.-Y. Li, M. Wang, PAN–PEO solid polymer electrolytes with high ionic conductivity, Mater. Chem. Phys. 89 (2005) 390–394, https://doi.org/10.1016/j.matchemphys.2004.09.032.
[35] L. Porcarelli, M.A. Aboudzadeh, L. Rubatat, J.R. Nair, A.S. Shaplov, C. Gerbaldi, D. Mecerreyes, Single-ion triblock copolymer electrolytes based on poly(ethylene oxide) and methacrylic sulfonamide blocks for lithium metal batteries, J. Power Sources. 364 (2017) 191–199, https://doi.org/10.1016/j.jpowsour.2017.08.023.
[36] C. Zuo, G. Chen, Y. Zhang, H. Gan, S. Li, L. Yu, X. Zhou, X. Xie, Z. Xue, Poly (ε-caprolactone)-block-poly(ethylene glycol)-block-poly(ε-caprolactone)-based hybrid polymer electrolyte for lithium metal batteries, J. Memb. Sci. 607 (2020) 118132, https://doi.org/10.1016/j.memsci.2020.118132.
[37] L. Ionescuvasii, B. Garcia, M. Armand, Conductivities of electrolytes based on PEI-b-PEO-b-PEI triblock copolymers with lithium and copper TFSI salts, Solid State Ionics. 177 (2006) 885–892, https://doi.org/10.1016/j.ssi.2006.01.024.
[38] T.-C. Wang, C.-Y. Tsai, Y.-L. Liu, Solid polymer electrolytes based on cross-linked polybenzoxazine possessing poly(ethylene oxide) segments enhancing cycling performance of lithium metal batteries, ACS Sustain. Chem. Eng. 9 (2021) 6274–6283, https://doi.org/10.1021/acssuschemeng.0c09230.
[39] L. Chen, Y. Guo, T. Fu, H.-B. Zhao, X.-L. Wang, Y.-Z. Wang, Targeted copolymerization in amorphous regions for constructing crystallizable functionalized copolymers, Macromolecules. 54 (2021) 4412–4422, https://doi.org/10.1021/acs.macromol.1c00469.
[40] D.J. Liaw, K.L. Wang, Y.C. Huang, K.R. Lee, J.Y. Lai, C.S. Ha, Advanced polyimide materials: Syntheses, physical properties and applications, Prog. Polym. Sci. 37 (2012) 907–974, https://doi.org/10.1016/j.progpolymsci.2012.02.005.
[41] Y. Zhuang, J.G. Seong, Y.M. Lee, Polyimides containing aliphatic/alicyclic segments in the main chains, Prog. Polym. Sci. 92 (2019) 35–88, https://doi.org/10.1016/J.PROGPOLYMSCI.2019.01.004.
[42] G. Vaganov, E. Ivan'kova, A. Didenko, E. Popova, V. Smirnova, V. Elokhovskiy, V. Yudin, Comparison of properties of carbon reinforced plastic obtained on the basis of semicrystalline polyimide <scp>R-BAPB</scp> and other high-temperature-resistant thermoplastic matrices, J. Appl. Polym. Sci. 140 (2023), https://doi.org/10.1002/app.54283.
[43] Z. Lan, C. Li, Y. Yu, J. Wei, Colorless semi-alicyclic copolyimides with high thermal stability and solubility, Polymers (Basel). 11 (2019) 1319, https://doi.org/10.3390/polym11081319.
[44] A.E. Soldatova, R.N. Shamsutdinova, T.V. Plisko, K.S. Burts, A.Y. Tsegelskaya, D. A. Khanin, K.Z. Monakhova, T.S. Kurkin, A.V. Bildyukevich, A.A. Kuznetsov, Synthesis of aromatic polyimides based on 3,4′-oxydianiline by one-pot polycondensation in molten benzoic acid and their application as membrane materials for pervaporation, Materials (Basel). 15 (2022) 6845, https://doi.org/10.3390/ma15196845.
[45] M. Zhang, L. Wang, H. Xu, Y. Song, X. He, Polyimides as promising materials for lithium-ion batteries: a review, Nano-Micro Lett. 15 (2023) 135, https://doi.org/10.1007/s40820-023-01104-7.
[46] Z. Song, H. Zhan, Y. Zhou, Polyimides: promising energy-storage materials, Angew. Chemie Int. Ed. 49 (2010) 8444–8448, https://doi.org/10.1002/ANIE.201002439.
[47] J.S. Kim, W. Choi, K.Y. Cho, D. Byun, J. Lim, J.K. Lee, Effect of polyimide binder on electrochemical characteristics of surface-modified silicon anode for lithium ion batteries, J. Power Sources. 244 (2013) 521–526, https://doi.org/10.1016/j.jpowsour.2013.02.049.
[48] G. Hernández, N. Lago, D. Shanmukaraj, M. Armand, D. Mecerreyes, Polyimide-polyether binders–diminishing the carbon content in lithium sulfur batteries, Mater. Today Energy. 6 (2017) 264–270, https://doi.org/10.1016/j.mtener.2017.11.001.
[49] Z. Lu, F. Sui, Y.-E. Miao, G. Liu, C. Li, W. Dong, J. Cui, T. Liu, J. Wu, C. Yang, Polyimide separators for rechargeable batteries, J. Energy Chem. 58 (2021) 170–197, https://doi.org/10.1016/j.jechem.2020.09.043.
[50] G. Hernández, N. Casado, R. Coste, D. Shanmukaraj, L. Rubatat, M. Armand, D. Mecerreyes, Redox-active polyimide–polyether block copolymers as electrode materials for lithium batteries, RSC Adv. 5 (2015) 17096–17103, https://doi.org/10.1039/C4RA15976D.
[51] G. Hernández, N. Casado, A.M. Zamarayeva, J.K. Duey, M. Armand, A.C. Arias, D. Mecerreyes, Perylene polyimide-polyether anodes for aqueous all-organic polymer batteries, ACS Appl. Energy Mater. 1 (2018) 7199–7205, https://doi.org/10.1021/acsaem.8b01663.
[52] T. Kim, J. Lee, N. Kim, S. Lee, M. Gu, B.S. Kim, Redox-active polyimides for energy conversion and storage: from synthesis to application, Chem. Commun. 59 (2022) 153–169, https://doi.org/10.1039/d2cc05660g.
[53] J. Zhang, Q. Lu, J. Fang, J. Wang, J. Yang, Y. NuLi, Polyimide encapsulated lithium-rich cathode material for high voltage lithium-ion battery, ACS Appl. Mater. Interfaces. 6 (2014) 17965–17973, https://doi.org/10.1021/am504796n.
[54] T. Watanabe, Y. Inafune, M. Tanaka, Y. Mochizuki, F. Matsumoto, H. Kawakami, Development of all-solid-state battery based on lithium ion conductive polymer nanofiber framework, J. Power Sources. 423 (2019) 255–262, https://doi.org/10.1016/j.jpowsour.2019.03.066.
[55] T. Shimane, T. Watanabe, N. Yokota, F. Matsumoto, M. Tanaka, H. Kawakami, Secondary battery performance of solid polymer electrolyte membranes based on lithium ion conductive polyimide nanofibers, J. Photopolym. Sci. Technol. 33 (2020) 321–325, https://doi.org/10.2494/photopolymer.33.321.
[56] Z. Li, Y. Liu, X. Liang, M. Yu, B. Liu, Z. Sun, W. Hu, G. Zhu, A single-ion gel polymer electrolyte based on polyimide grafted with lithium 3-chloropropanesulfonyl (trifluoromethanesulfonyl) imide for high performance lithium ion batteries, J. Mater. Chem. A. 11 (2022) 1766–1773, https://doi.org/10.1039/d2ta09097j.
[57] P. Wang, L. Wang, X. Liang, Y. You, Z. Li, Y. Liu, B. Liu, Z. Sun, W. Hu, Single-ion gel polymer electrolyte based on in-situ UV irradiation cross-linked polyimide complexed with PEO for lithium-ion batteries, Macromol. Rapid Commun. 44 (2023) 2200865, https://doi.org/10.1002/marc.202200865.
[58] M. Higa, K. Yaguchi, R. Kitani, All solid-state polymer electrolytes prepared from a graft copolymer consisting of a polyimide main chain and poly(ethylene oxide) based side chains, Electrochim. Acta. 55 (2010) 1380–1384, https://doi.org/10.1016/j.electacta.2009.07.046.
[59] L. Matesanz-Niño, M.T. Webb, A. González-Ortega, L. Palacio, C. Álvarez, Á. E. Lozano, M. Galizia, Plasticization resistant gas separation membranes derived from polyimides exhibiting polyethylene-oxide moieties, Polymer (Guildf). 290 (2024) 126535, https://doi.org/10.1016/j.polymer.2023.126535.
[60] L. Matesanz-Niño, C. Aguilar-Lugo, P. Prádanos, A. Hernandez, C. Bartolomé, J. G. de la Campa, L. Palacio, A. González-Ortega, M. Galizia, C. Álvarez, Á.E. Lozano, Gas separation membranes obtained by partial pyrolysis of polyimides exhibiting

polyethylene oxide moieties, Polymer (Guildf). 247 (2022) 124789, https://doi.org/10.1016/j.polymer.2022.124789.
[61] I. Butnaru, A.-P.-P. Chiriac, C. Tugui, M. Asandulesa, M.-D.-D. Damaceanu, The synergistic effect of nitrile and jeffamine structural elements towards stretchable and high-: K neat polyimide materials, Mater. Chem. Front. 5 (2021) 7558–7579, https://doi.org/10.1039/d1qm00643f.
[62] E. Woo, E. Coletta, A. Holm, J. Mun, M.F. Toney, D.Y. Yoon, C.W. Frank, Polyimide-PEG Segmented Block Copolymer Membranes with High Proton Conductivity by Improving Bicontinuous Nanostructure of Ionic Liquid-Doped Films, Macromol. Chem. Phys. 220 (2019) 1–8, https://doi.org/10.1002/macp.201900006.
[63] E. Coletta, M.F. Toney, C.W. Frank, Influences of liquid electrolyte and polyimide identity on the structure and conductivity of polyimide-poly(ethylene glycol) materials, J. Appl. Polym. Sci. 132 (2015) 1–13, https://doi.org/10.1002/app.41675.
[64] E. Coletta, M.F. Toney, C.W. Frank, Effects of aromatic regularity on the structure and conductivity of polyimide-poly(ethylene glycol) materials doped with ionic liquid, J. Polym. Sci. Part B Polym. Phys. 53 (2015) 509–521, https://doi.org/10.1002/polb.23664.
[65] A.A. Kuznetsov, One-pot polyimide synthesis in carboxylic acid medium, High Perform. Polym. 12 (2000) 445–460, https://doi.org/10.1088/0954-0083/12/3/307.
[66] A.M. Orlova, A.Y. Alentiev, T.I. Kolesnikov, A.Y. Tsegelskaya, K.Z. Monakhova, S. V. Chirkov, R.Y. Nikiforov, I.G. Abramov, A.A. Kuznetsov, Novel organo-soluble poly(ether imide)s based on diethyltoluenediamine: Synthesis, characterization and gas transport properties, Polymer (Guildf). 256 (2022) 125258, https://doi.org/10.1016/j.polymer.2022.125258.
[67] T.I. Kolesnikov, A.M. Orlova, F.V. Drozdov, A.I. Buzin, G.V. Cherkaev, A. S. Kechekyan, P.V. Dmitryakov, S.I. Belousov, A.A. Kuznetsov, New imide-based thermosets with propargyl ether groups for high temperature composite application, Polymer (Guildf). 254 (2022) 125038, https://doi.org/10.1016/j.polymer.2022.125038.
[68] D. Devaux, R. Bouchet, D. Glé, R. Denoyel, Mechanism of ion transport in PEO/LiTFSI complexes: effect of temperature, molecular weight and end groups, Solid State Ionics. 227 (2012) 119–127, https://doi.org/10.1016/j.ssi.2012.09.020.
[69] C.-K. Ku, Y.-D. Lee, Microphase separation in amorphous poly(imide siloxane) segmented copolymers, Polymer (Guildf). 48 (2007) 3565–3573, https://doi.org/10.1016/j.polymer.2007.04.028.
[70] E. Giannetti, Thermal stability and bond dissociation energy of fluorinated polymers: a critical evaluation, J. Fluor. Chem. 126 (2005) 623–630, https://doi.org/10.1016/j.jfluchem.2005.01.008.
[71] L. Stolz, S. Röser, G. Homann, M. Winter, J. Kasnatscheew, Pragmatic approaches to correlate between the physicochemical properties of a linear poly(ethylene oxide)-based solid polymer electrolyte and the performance in a high-voltage Li-Metal battery, J. Phys. Chem. c. 125 (2021) 18089–18097, https://doi.org/10.1021/acs.jpcc.1c03614.
[72] A. Gupta, E. Kazyak, N. Craig, J. Christensen, N.P. Dasgupta, J. Sakamoto, Evaluating the effects of temperature and pressure on Li/PEO-LiTFSI Interfacial stability and kinetics, J. Electrochem. Soc. 165 (2018) A2801–A2806, https://doi.org/10.1149/2.0901811jes.
[73] C.A. Angell, C. Liu, E. Sanchez, Rubbery solid electrolytes with dominant cationic transport and high ambient conductivity, Nature. 362 (1993) 137–139, https://doi.org/10.1038/362137a0.
[74] H. Li, Y. Du, X. Wu, J. Xie, F. Lian, Developing “polymer-in-salt” high voltage electrolyte based on composite lithium salts for solid-state li metal batteries, Adv. Funct. Mater. 31 (2021), https://doi.org/10.1002/adfm.202103049.
[75] J. Zhang, Y. Zeng, Q. Li, Z. Tang, D. Sun, D. Huang, L. Zhao, Y. Tang, H. Wang, Polymer-in-salt electrolyte enables ultrahigh ionic conductivity for advanced solid-state lithium metal batteries, Energy Storage Mater. 54 (2023) 440–449, https://doi.org/10.1016/j.ensm.2022.10.055.
[76] M. Forsyth, J. Sun, D.R. Macfarlane, A.J. Hill, Compositional dependence of free volume in PAN/LiCF3SO3 polymer-in-salt electrolytes and the effect on ionic conductivity, J. Polym. Sci. Part B Polym. Phys. 38 (2000) 341–350, https://doi.org/10.1002/(SICI)1099-0488(20000115)38:2<341::AID-POLB6>3.0.CO;2-S.
[77] X. Wang, F. Chen, G.M.A. Girard, H. Zhu, D.R. MacFarlane, D. Mecerreyes, M. Armand, P.C. Howlett, M. Forsyth, Poly(Ionic Liquid)s-in-salt electrolytes with co-coordination-assisted lithium-ion transport for safe batteries, Joule. 3 (2019) 2687–2702, https://doi.org/10.1016/j.joule.2019.07.008.
[78] F. Chen, X. Wang, M. Armand, M. Forsyth, Cationic polymer-in-salt electrolytes for fast metal ion conduction and solid-state battery applications, Nat. Mater. 21 (2022) 1175–1182, https://doi.org/10.1038/s41563-022-01319-w.
[79] B.V. Kotov, T.A. Gordina, V.S. Voishchev, O.V. Kolninov, A.N. Pravednikov, Aromatic polyimides as charge transfer complexes, Polym. Sci. U.S.S.R. 19 (1977) 711–716, https://doi.org/10.1016/0032-3950(77)90131-9.
[80] Y. Watanabe, Y. Ugata, K. Ueno, M. Watanabe, K. Dokko, Does Li-ion transport occur rapidly in localized high-concentration electrolytes? Phys. Chem. Chem. Phys. 25 (2023) 3092–3099, https://doi.org/10.1039/D2CP05319E.
[81] J. Evans, C.A. Vincent, P.G. Bruce, Electrochemical measurement of transference numbers in polymer electrolytes, Polymer (Guildf). 28 (1987) 2324–2328, https://doi.org/10.1016/0032-3861(87)90394-6.
[82] K. Pożyczka, M. Marzantowicz, J.R. Dygas, F. Krok, IONIC conductivity and lithium transference number of poly(ethylene oxide):LiTFSI system, Electrochim. Acta. 227 (2017) 127–135, https://doi.org/10.1016/j.electacta.2016.12.172.
[83] M. Sun, Z. Zeng, W. Zhong, Z. Han, L. Peng, C. Yu, S. Cheng, J. Xie, In situ prepared “polymer-in-salt” electrolytes enabling high-voltage lithium metal batteries, J. Mater. Chem. A. 10 (2022) 11732–11741, https://doi.org/10.1039/D2TA00093H.
[84] Y. Sun, X. Zhang, C. Ma, N. Guo, Y. Liu, J. Liu, H. Xie, Fluorine-containing triblock copolymers as solid-state polymer electrolytes for lithium metal batteries, J. Power Sources. 516 (2021) 230686, https://doi.org/10.1016/j.jpowsour.2021.230686.
[85] D.H.C. Wong, J.L. Thelen, Y. Fu, D. Devaux, A.A. Pandya, V.S. Battaglia, N. P. Balsara, J.M. DeSimone, Nonflammable perfluoropolyether-based electrolytes for lithium batteries, Proc. Natl. Acad. Sci. 111 (2014) 3327–3331, https://doi.org/10.1073/pnas.1314615111.
[86] I. Aldalur, M. Martinez-Ibañez, A. Krztoń-Maziopa, M. Piszcz, M. Armand, H. Zhang, Flowable polymer electrolytes for lithium metal batteries, J. Power Sources. 423 (2019) 218–226, https://doi.org/10.1016/j.jpowsour.2019.03.057.
[87] J.-P. Gu, K.-Y. Zhang, X.-T. Li, J. Dong, Q.-H. Zhang, X. Zhao, Construction of safety and non-flammable polyimide separator containing carboxyl groups for advanced fast charing lithium-ion batteries, Chinese J. Polym. Sci. 40 (2022) 345–354, https://doi.org/10.1007/s10118-022-2678-4.
[88] X. Luo, X. Lu, X. Chen, Y. Chen, C. Song, C. Yu, N. Wang, D. Su, C. Wang, X. Gao, G. Wang, L. Cui, A robust flame retardant fluorinated polyimide nanofiber separator for high-temperature lithium–sulfur batteries, J. Mater. Chem. A. 8 (2020) 14788–14798, https://doi.org/10.1039/D0TA00439A.
[89] R. Andersson, G. Hernández, J. See, T.D. Flaim, D. Brandell, J. Mindemark, Designing Polyurethane Solid Polymer Electrolytes for High-Temperature Lithium Metal Batteries, ACS Appl. Energy Mater. 5 (2022) 407–418, https://doi.org/10.1021/acsaem.1c02942.
[90] I. Aldalur, H. Zhang, M. Piszcz, U. Oteo, L.M. Rodriguez-Martinez, D. Shanmukaraj, T. Rojo, M. Armand, Jeffamine® based polymers as highly conductive polymer electrolytes and cathode binder materials for battery application, J. Power Sources. 347 (2017) 37–46, https://doi.org/10.1016/j.jpowsour.2017.02.047.
[91] R. Andersson, I.L. Johansson, K.I. Shivakumar, G. Hernández, Y. Inokuma, J. Mindemark, Implementation of highly crystalline polyketones as solid polymer electrolytes in high-temperature lithium metal batteries, Solid State Ionics. 410 (2024) 116542, https://doi.org/10.1016/j.ssi.2024.116542.
[92] I.L. Johansson, D. Brandell, J. Mindemark, Mechanically stable UV-crosslinked polyester-polycarbonate solid polymer electrolyte for high-temperature batteries, Batter. Supercaps. 3 (2020) 527–533, https://doi.org/10.1002/batt.201900228.